Journal of Radioanalytical and Nuclear Chemistry (2025) 334:7097–7106
https://doi.org/10.1007/s10967-025-10393-8

Feasibility study of a neutron-based method for field measurement of chloride in concrete

H. H. Chen-Mayer[1] · S. F. Hoogerheide[1] · A. Ashfaq[2] · J. M. LaManna[1] · S. Z. Jones[1] · M. Al-Sheikhly[2] · R. L. Livingston[2]

Received: 8 July 2025 / Accepted: 5 September 2025 / Published online: 30 September 2025

Abstract
Sub-percent levels of chloride in concrete is known to promote corrosion of the interior metal reinforcement which leads to structural degradation. The current industrial practice of chloride analysis through destructive chemical processes can be augmented by on-site non-destructive techniques such as prompt gamma activation analysis (PGAA), which can measure Cl along with Si and Ca in bulk concrete. PGAA commonly performed in a nuclear reactor is not suitable for field work. We tested a portable neutron generator based PGAA system for measuring Cl in a set of 90 cm × 90 cm × 12.7 cm concrete slabs in a laboratory setting. The measured results were compared to Monte Carlo radiation transport simulated gamma-ray spectral response as a function of Cl mass fraction. This work serves as feasibility study for a field-deployable "chloride sensor" for concrete structures, providing useful information for future effort in improving the detection limit and in designing robust detection and quantification methods.

Keywords Chloride · Corrosion in concrete · Infrastructure monitoring · PGAA · Elemental analysis

Introduction

Prompt gamma activation analysis (PGAA) is a neutron based non-destructive technique for quantitative composition analysis of bulk materials. It can be used for the simultaneous determination of major, minor, and trace levels of elements, often in the form of mass ratio to a major element [1, 2]. Isotope-specific prompt gamma rays are emitted by de-excitation of an unstable nucleus upon capturing a thermal neutron. PGAA is commonly performed in a nuclear reactor where a thermal or cold neutron beam is delivered to a sample for analysis [3, 4]. The gamma rays are recorded by an energy-resolved spectrometer viewing the sample.

The extensive use of Portland cement concrete in constructing highways is being endangered by the corrosion of reinforcing steel, which is significantly hastened by the penetration of chloride ions [5, 6]. The primary sources of these chloride ions include de-icing salts and/or the use of seawater as part of the concrete mix water or as airborne droplets from ocean spray. The development of a neutron-based method for field measurement of chloride in concrete could potentially revolutionize how we detect and mitigate such corrosion, thereby safeguarding our infrastructure investments and ensuring their longevity and safe operations.

The current standard testing methods for chloride measurement, while widely used, have several significant limitations. They involve using a rotary hammer to remove a sample from the structure, which is destructive and does not permit repeated measurements at the same points over time. The sample is then pulverized and treated with nitric acid to extract the chloride. Titration methods in wet chemistry are utilized to determine chloride concentration [7, 8]. Alternatively, the chloride solution can be analyzed using a selective electrode or atomic absorption spectroscopy [9]. These traditional methods are limited in their ability to analyze structures with nonhomogeneous chloride depositions and cannot easily create a chloride profile based on depth. These limitations spawned other new, non-destructive approaches, such as electrical resistivity, ion selective electrode and optical fiber sensors [10].

✉ H. H. Chen-Mayer
chen-mayer@nist.gov

[1] National Institute of Standards and Technology, Gaithersburg, MD 20899, USA

[2] University of Maryland, College Park, MD 20742, USA

Prompt gamma activation analysis (PGAA) presents a practical and nondestructive alternative for on-site measurements. Neutrons, capable of penetrating several feet of concrete, can interact with various elements within the bulk. A stable nucleus of an element can capture a low-energy neutron and be excited several MeV above its ground state. It then rapidly (within 10^{-14} s to 10^{-9} s) de-excites by emitting characteristic gamma rays. Most elements can be detected using this principle, with detection limits dependent on the element's neutron capture cross-section, gamma-ray yield, and abundance in the material. The reaction ^{35}Cl(n, γ)^{36}Cl produces numerous prompt gamma-ray lines suitable for PGAA measurements [11]. Figure 1 shows the major gamma rays produced in the de-excitation of the ^{36}Cl nucleus from one of the excited nuclear levels [12]. The line at 6110 keV, with combined neutron capture and gamma yield cross-sections (partial gamma cross section) of 6.59 b [13], plays an essential role in detecting chloride in concrete. This is because it is at sufficiently high energy to avoid strong gamma-ray self-shielding by the bulk material, and its peak position on the energy spectrum has little interference from other peaks.

The net area per unit count time (count rate) $C(E_\gamma)$ for a given photopeak at energy E_γ in the prompt gamma-ray spectrum is related to the neutron capture and gamma-ray emission probabilities of the corresponding isotope, which, by its known natural abundance in an element, is related to the number of atoms for the element by this simplified equation [13]:

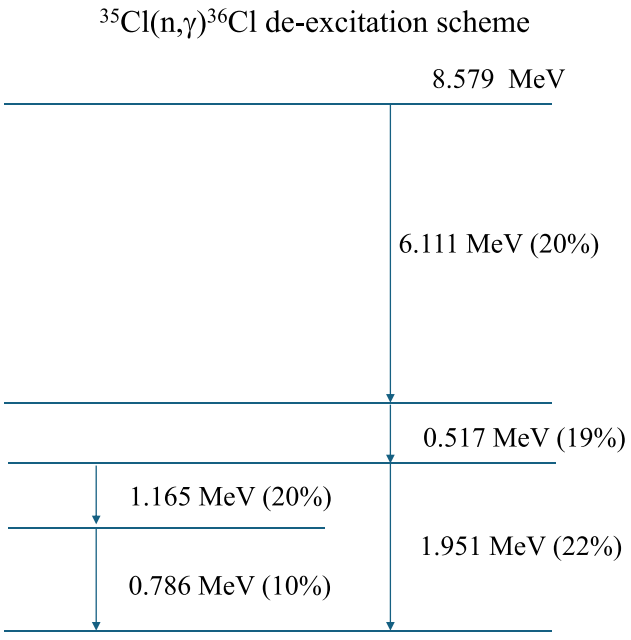

Fig. 1 Prompt gamma emissions for the excited ^{36}Cl nucleus [12]

$$C(E_\gamma) = \phi_n N_Z \varepsilon_{E_\gamma} \sigma_\gamma^Z(E_\gamma) \quad (1)$$

where $\sigma_\gamma^Z(E_\gamma)$ is the thermal neutron partial gamma cross section of element Z at gamma-ray energy E_γ (in the case of Cl, for the $E_\gamma = 6110$ keV transition, $\sigma_\gamma^Z(E_\gamma) = 6.59$b), ε_{E_γ} is the detector absolute efficiency at the peak energy E_γ, N_Z is the number of atoms of the element irradiated by the neutron beam, ϕ_n is the thermal equivalent neutron flux.

Nuclear reactor-based facilities can perform PGAA of Cl in concrete at a smaller scale (a few g of sample at a cm scale), for example, studies of small pellets made from crushed powder [14] and of intact 5 cm diameter cylinders [15]. However, for on-site analysis, it is necessary to use neutron sources from compact neutron generators or radioactive sources, which are portable for field measurements. An instance of using a proton linear accelerator to bombard a thick beryllium (Be) target, which in turn generates the neutrons via the ^{9}Be(p,n)^{9}B reaction, was also reported [16, 17]. With the proper shielding (e.g., lead cages) engineered in place, these techniques promise to replace traditional chloride measurement methods.

There were previous works on PGAA for Cl in concrete, for example, using a ^{241}AmBe neutron source (average neutron energy 4.2 MeV) with a paraffin moderator [18], and a ^{252}Cf neutron source (average neutron energy 2 MeV) with a polyethylene moderator [19–22]. (These fast neutron energies are comparable to the 2.45 MeV monoenergetic neutrons used in the current work.) The gamma rays were detected using a high-purity germanium (HPGe) gamma-ray detector. This type of radioactive neutron source could raise security and safety concerns in field deployment.

For this work, we investigate the feasibility of using neutrons from a portable deuterium-deuterium (DD) neutron generator for PGAA of a large concrete slab for possible future field deployment, relevant to in-situ inspection of infrastructures. Specifically, we focus on measuring the chloride content in the concrete slab for corrosion prediction. A suite of concrete slabs with five different levels of chloride concentration was cast for testing in a previous work [23]. There have been other experimental works in this topic [24–27], but with the detector either behind the concrete or at an angle off the edge, and none were performed with the same-side geometry, where both the neutron source and the detector are on the same surface of the concrete. Our set-up better resembles the typical field situation in which getting behind the structure is impractical. Furthermore, we replaced the HPGe detector with a $LaBr_3$ scintillator detector, which has the advantage of room temperature operations (no liquid nitrogen cooling required), and greater efficiency (higher count rate), at the expense of energy resolution.

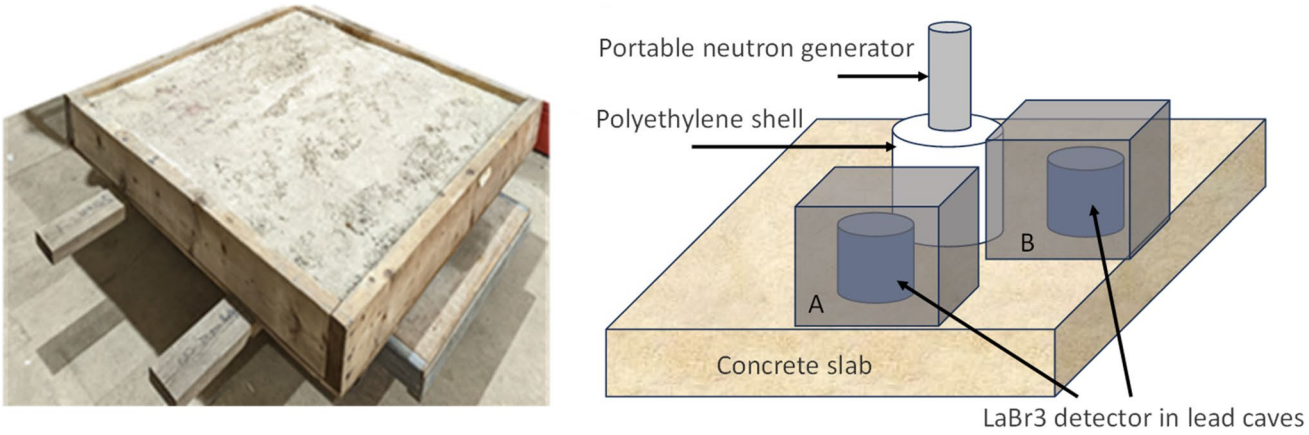

Fig. 2 Left: photograph of one of the five concrete slabs in wooden box fame on a cart for measurement. The nominal dimensions are 90 cm × 90 cm × 12.7 cm excluding the frame. Each slab contains a different amount of added chloride. Right: schematic sketch of the experimental setup, with the neutron source and detectors on the same side of the concrete slab, and the fast neutrons from the generator are thermalized inside the concrete slab, inducing prompt gamma-ray emission

Materials and methods

Concrete material

Five concrete slabs of the same base composition but with different levels of chloride were cast at the University of Maryland for another study [23]. The highest Cl content by mass is 0.6%. Figure 2 shows the photo of one of the slabs, with a dimension of about 90 cm × 90 cm × 12.7 cm thick, inside a wooden frame. The nominal intended composition is listed in Table 1. The resulting prompt gamma-ray spectrum was measured using two large volume $LaBr_3$ detectors. The configuration of the measurement is shown in Fig. 2 schematically. The bottom of the neutron generator housing is within a cm from the slab surface. As indicated by MCNP simulation, the concrete slab acts as a fast neutron moderator to produce thermal neutrons that are useful for capture gamma rays from the elements inside the concrete.

Monte Carlo simulation

The measurement system and the gamma-ray spectrum obtained in the detector were investigated using a general-purpose Monte Carlo N-Particle (MCNP) code [28]. The layout shown in Fig. 2 was used in the geometrical model. The nominal composition for concrete based on the portions of Si and Ca derived from the mix shown in Table 1, with sand (SiO_2) as fine aggregate, and sand, limestone ($CaCO_3$), dolomite [$CaMg(CO_3)_2$], and granite (70%SiO_2, 1.8%CaO) as coarse aggregate. The mass fractions of Si and Ca in concrete based on the mix recipe are determined as follows:

$$\begin{pmatrix} \frac{\text{Si}}{\text{concrete}} \\ \frac{\text{Ca}}{\text{concrete}} \end{pmatrix} = \begin{pmatrix} \frac{\text{cement paste}}{\text{concrete}} & \frac{\text{fine}}{\text{concrete}} & \frac{\text{coarse}}{\text{concrete}} \end{pmatrix} \begin{pmatrix} \frac{\text{Si}}{\text{cement paste}} & \frac{\text{Ca}}{\text{cement paste}} \\ \frac{\text{Si}}{\text{fine}} & \frac{\text{Ca}}{\text{fine}} \\ \frac{\text{Si}}{\text{coarse}} & \frac{\text{Ca}}{\text{coarse}} \end{pmatrix}$$

The four types of concrete with increasing Cl mass fraction (converted to atom fraction) were simulated. The $LaBr_3$ detector with a nominal energy dependent full width at half maximum was assumed, and a pulse high spectrum of the prompt gamma rays was obtained using the F8 tally.

Measurement system

The neutron generator used in this work is a Thermo Electron Corporation P325 DD neutron generator,[1] housed in the NIST Californium Neutron Irradiation Facility (CNIF). The CNIF is composed of a large experiment room with concrete walls, floor, and ceiling, inside of which is a smaller room whose walls, floor, and ceiling are composed of anhydrous borax inside a thin aluminum shell. This inner room of anhydrous borax prevents neutrons that are scattered from the concrete walls from returning to the source and sample. A smaller control room, shielded from the neutron radiation, houses the computers and electronics, connected via 25 m of cable.

The DD neutron generator produces neutrons at an energy of 2.45 MeV. The generator head is a cylinder that is 70 cm long and 10 cm diameter. It operates at a beam current of 20–110 μA and a voltage of 40–110 kV. The output of

[1] Identification of a product herein is for documentation purposes only, and does not imply recommendation or endorsement by NIST, nor does it imply that this product is necessarily the best available for the purpose.

Table 1 Nominal concrete mix parameters and Cl mass fractions in the slabs (from [22])

Ingredient	Mass (kg)
Water	30
Cement	60
Coarse aggregate	137
Fine aggregate	122
Mix total	348
Slab number	Nominal Cl mass fraction
1	0.006
2	0.005
3	0.003
4	0.00025
Control	0

the generator is not calibrated, although the output scales roughly linearly with beam current and exponentially with high voltage, according to the manufacturer, with a maximum neutron output on the order of 10^6 per second into 4π. (Note that the prompt gamma production is proportional to the power of the generator, and better sensitivity can be achieved by using a more powerful generator.) The generator can be operated in both continuous and pulsed mode. For this work, the continuous mode was used. The generator was surrounded by a concentric cylindrical shell of high-density polyethylene, placed vertically with the end of the cylinder placed directly on the center of the top surface of the concrete slab.

A cylindrical (9 cm diameter × 19 cm height) $LaBr_3$ scintillator detector, controlled by a CAEN Hexagon 16 k multichannel analyzer and a Windows PC, was used for gamma spectrum acquisition. The channel to energy conversion follows a third order polynomial, calibrated using known energy peak locations. The detector and Pb shielding were placed near the edge of the top surface of the concrete slab, forming a same-side geometry, to simulate a field situation, where the neutron source and gamma detection must take place on the outside of a structure.

Data reduction

For prompt gamma spectral analysis, the peak of interest, Cl at 6110 keV, is a response to the amount of Cl in concrete. In practice, major elements in the concrete matrix, Si and Ca, with a peak at 4934 and 6420 keV, respectively, may be used for internal ratio, which, as shown in Eq. (1), eliminates the need for knowing the neutron flux which is attenuated by the concrete but affects all the elements the same way, leaving only the ratio of molar atoms weighted by the gamma-ray cross sections and detector efficiency. For bulk samples such as the large concrete slab, gamma-ray attenuation depends on the energy, these effects can be estimated. While ε_{Cl} may be different from ε_{Si} and ε_{Ca}, in the range of 5–6 MeV, the efficiency for the $LaBr_3$ is assumed to be flat. This is assumed for the MCNP simulation.

The mass fractions of Si and Ca vary greatly by the type of aggregates used in the concrete mix and by the local uniformity, but the sum of the two are less varied. For the concrete mix proportions shown in Table 1, a compilation of the four commonly used types of materials for fine and coarse aggregates, namely, sand, limestone, granite, dolomite (with 16 total combinations), shows that the average mass fraction and coefficient of variation (COV = standard deviation/mean × 100%) for Si, Ca, and for (Si + Ca) are: 0.16 (COV 65%), 0.19 (COV 46%), and 0.36 (COV 14%), respectively. Therefore, if the peak count of Cl is ratioed to the sum of that of Si and Ca, the response is a more robust representation of Cl mass fraction in concrete regardless the types of aggregates in the original mix, which may not be known in the field. For this study, the counts ratio of Cl/(Si + Ca) is used as a measure of the response to the Cl mass fraction in concrete, for both MCNP simulation and measurement. The peak areas were estimated by peak integration software PeakEasy [29]. The subsequent data processing and plotting were carried out by custom python code.

Results and discussion

Results of MCNP simulation

To visualize the spatial non-uniformity of the neutron and gamma distributions inside the slab, mesh tallies created from the simulation were processed [30] for neutron and gamma intensities everywhere within the slab. A few 2D slices are shown in Fig. 3. The neutron map by energy region represented by relative intensity shows that the thermalized component is far lower than fast neutrons. The neutron flux decreases by three orders of magnitude from the center to the end of the slab in the x–y directions, and by five orders of magnitude as a function of depth in the x–z plane. The corresponding gamma map is also shown. Given the highly non-uniform neutron and gamma fields, the signal at the detector is the bulk average of all the gamma rays arriving within the solid angle after attenuation by the material in the path.

The model includes the pulse height spectrum from the $LaBr_3$ detector. The detectors were placed symmetrically on the slab with respect to the neutron source, and assumed to be identical in terms of solid angle and detection efficiency, and therefore only the pulse height spectrum from one detection was tallied. For each of the four types of aggregates, a prompt gamma spectrum was produced from each Cl mass fraction (ranging from 1e-3 to 2e-2), and the intensity for the

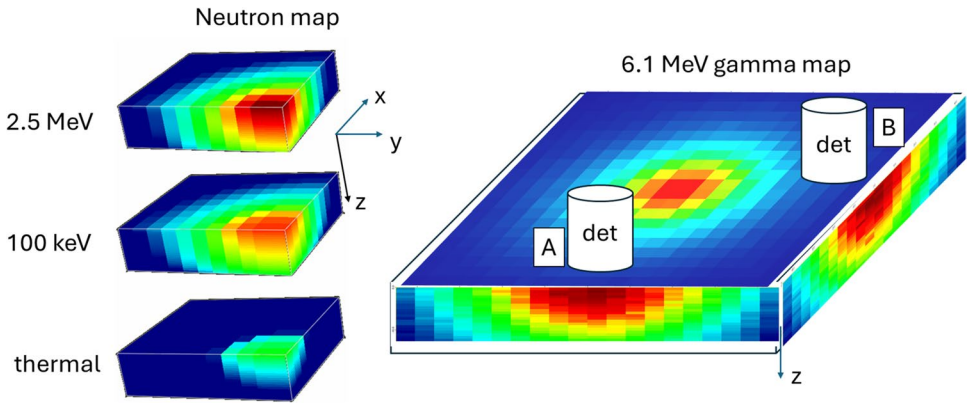

Fig. 3 Neutron (left) and gamma (right) maps by mesh tally inside the concrete slab by MCNP simulation, shown in false colors. For the neutron map, a quarter cutout of the 90 cm × 90 cm × 12.7 cm full slab is shown. Detector locations are indicated. The thermal component is responsible for capture gamma-ray production

3 peaks of interest (Cl at 6110 keV, Si at 4934 keV, and Ca at 6420 keV) were extracted and the counts ratio obtained. The select spectra for the granite aggregate group are shown in Fig. 4, together with the experimental spectra (discussed in the next section). The detector characteristics have not been fully modeled, as seen by the width of the peak. The model also does not include other structural supporting materials in the environment which might have caused the extra background and peaks.

The relative peak intensity (ratio) as a function of Cl mass fraction is compiled to produce a response curve, shown in Fig. 5a. It contains the simulated data for all four types of coarse aggregates. An average curve (by least squares fitting of all data points) is shown, and a 95% prediction interval (PI) is calculated based on the 95% confidence interval (CI)

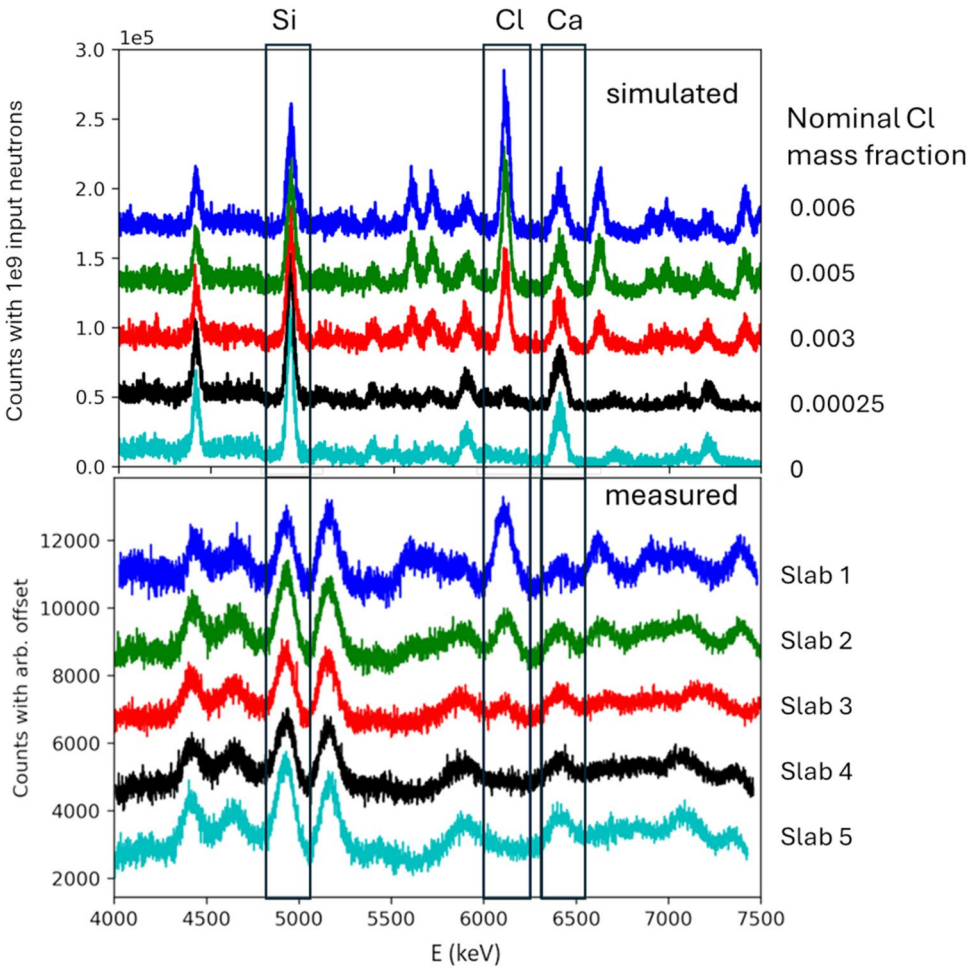

Fig. 4 Prompt gamma spectra from 5 levels of Cl concentration, simulated (top panel) and measured (bottom panel), in the region containing the peaks for Si (4934 keV), Cl (6110 keV) and Ca (6420 keV). For the simulated spectra, the Cl mass fractions are from 0 to 0.006, matching the nominal values of the slabs. The measured spectra are from the 5 concrete slabs, from top to bottom in descending order for Cl concentration, vertically displaced for clarity. Slab 3 was thinner than others; the amplitude is multiplied by 1.5 for the purpose of comparable display. The peak in the experimental spectra to the right of the Si peak does not appear in the simulated spectra, could be due to neutron reactions with the detector material. It is well separated from the Si peak and does not affect the results

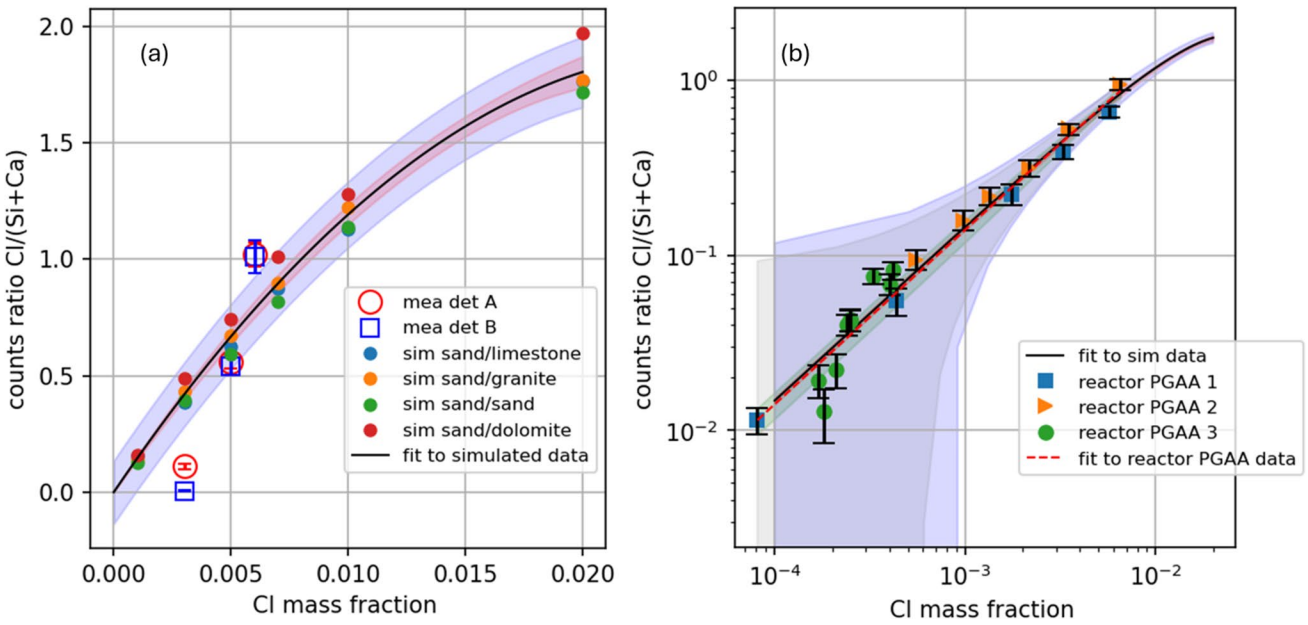

Fig. 5 **a** simulated data (for Cl mass fractions of 1e-3, 3e-3, 5e-3, 7e-3, 1e-2, 2e-2) for all four types of coarse aggregates (solid circles) and a quadratic fit (solid line), with the shaded band representing a 95% prediction interval (PI). The measured data from the two detectors for the first 3 slabs are shown as open circles and squares. **b** log–log plot of reactor based PGAA on gram sized pressed pellets of concrete powder at lower mass fractions form previous studies with the fit (dashed curve), which is indistinguishable from the fit to the simulated data for a large slab [replotted from (**a**), solid curve, extended to cover 1e-4]. The reactor PGAA data were obtained at the NIST cold neutron beam with thermal equivalent neutron flux of 10^9/cm^2-s on concrete powder pressed pellet samples (600 mg–1 g) with known Cl mass fractions, measurement time 1–1.5 h and counting statistical uncertainty < 1.5% for data sets 1 and 2, and < 8% for data set 3. The error bars assigned were based on the confidence intervals from the fit to all data points

of the fitted function and the residuals of the fit. This is shown as the shaded band along the fitted curve. The 95% PI at Cl mass fraction of 0.006 is about 18%. Therefore, even if the exact type of aggregate in the concrete is unknown, the ratio of Cl/(Si + Ca) can be expected to fall within this band, with about 18% uncertainty.

At higher Cl mass fractions, the curve appears to be saturating. This is not due to neutron attenuation due to higher Cl, because the ratio would remove that effect. Instead, it is due to the interference of a small Cl peak near the Si peak that is not separated from the Si peak due to the poor energy resolution. At lower Cl mass fractions it is negligible, but as the Cl increases, it starts contributing to the Si peak intensity and artificially lower the ratio of Cl/(Si + Ca). If a high resolution HPGe detector is used, the peaks can be separated, and the linearity is preserved. This is the trade-off between the convenience of a scintillator detector and the HPGe with cryocooling. However, as long as the simulation also includes the interference peak, the data should follow the trend. In the region of interest for corrosion threshold for which the Cl mass fraction is below 1%, the interference is considered negligible given the large uncertainty of the bulk composition.

Results of measurement

A prompt gamma-ray spectrum was collected for each slab using the same geometry and detector settings. The resolution of the $LaBr_3$ detector is nowhere near that of a HPGe detector, and therefore cannot resolve many peaks that are close together. Nevertheless, the main goal of identifying Cl using one of its peaks at 6110 keV is achievable above certain concentrations. To verify the measured 6110 keV was from Cl, a series of ¼″ × 2″ × 4″ (0.635 cm × 61 cm × 122 cm) polyvinylchloride (PVC, C_2H_3Cl) sheets was added incrementally on top of the concrete slab to ensure the peak increased with the number of sheets. The PVC sheets were then removed to commence the concrete measurement.

The two $LaBr_3$ detectors were placed on the surface of the slab (Fig. 2), 90 degrees from each other, measuring the prompt gamma spectrum simultaneously. Assuming radial symmetry in the uniformity of the field, the count rate ratios from the two detectors can be averaged to reduce the spatial inhomogeneity. Spectra from one of the detectors are shown in the lower panel of Fig. 4. The Cl signal is barely above background in the slab 3 spectrum, and not detectable in the slab 4 which is indistinguishable from the 5th spectrum from the control slab that had no Cl. The corresponding

simulation for slab 4 (top panel, nominal Cl mass fraction of 2.5e-4) also indicates lack of signal. The measurement time varied between 6 and 20 h. The 3rd slab appeared to have been less massive than others.

Discussion

From the acquired spectra, the relevant peak count rates and ratios were extracted and compiled in Table 2. These experimentally determined ratios are also plotted against the nominal Cl mass fraction in Fig. 5a, along with the simulated data. For slab 1 and 2, the count rate ratios of Cl to Si are the same for the two detectors, despite variations in the absolute counts. For slab 3, the uncertainty is too high in detector B to have a meaningful comparison. The count rate of the Si peak itself is comparable in both detectors for slab 1. For the rest of the slabs, the Si count rate in detector B is about half of that in detector A. As stated earlier, the location dependence of the absolute peak count rate is expected if the slab thickness and composition inhomogeneity are uneven, reflecting the real-world situation. By taking the count rate ratio of Cl to the sum of Si and Ca, such variation can be mitigated. As in the simulation section, the interference of a Cl peak near the Si peak is included in the analysis. The relative detection efficiency can vary depending on the measurement geometry, and difficult to calibrate given large sample volume in view. The detector efficiency in the range of 5–6.5 MeV was considered constant, same as for the simulation. The data point from detector B for slab 3 has high uncertainty and is inconsistent with detector A. Data from both detectors are way below the simulated curve, indicating less reliable detection at these levels. For the two higher levels, the measured values are closer to the simulated response. It is worth mentioning that the nominal Cl mass fractions in the slabs also have uncertainty depending on the casting conditions, adding a reasonable 15% horizontal error bars could bring the highest point into the 95% PI zone.

For reference, the counts ratio of Cl/(Si + Ca) was extracted from 3 sets of previously acquired PGAA data (set 1 and 2 from unpublished report, set 3 from [14]) on small powdered concrete samples using HPGe at a reactor neutron beam. Because the capture flux is more than 2 orders of magnitude higher in a reactor-based facility than in the portable neutron generator, the measured Cl mass fraction extends to the 1e-4 region (Fig. 5b, log–log plot to magnify the lower region). The counts ratios are plotted against the known Cl mass fractions, and fitted together by least squares with the same quadratic function, yielding a 95% PI of 12% at Cl mass fraction of 0.006, lower than the 18% for the slab simulation. The fitted curve for the simulation in Fig. 5a is also plotted in Fig. 5b. The overlapping of the two fitted curves—that for the simulated response for the bulk slab, with that of standard small pellet data from reactor PGAA measurement—suggests a robustness of the internal ratio method at Cl mass fraction in the sub-percent region, for vastly different neutron source, geometry and sample size.

Based on the measured spectra from the two highest Cl mass fraction (6e-3 and 5e-3), using this criteria (Glenn Knoll): MDL $\approx 2L_c + k_{1-\alpha}^2$ where $L_c = \sqrt{2}k_{1-\alpha}\sigma_{N_B}$, $k_{1-\alpha} = 1.645$ is the coverage factor of 95% confidence, and $\sigma_{N_B} = \sqrt{N_B}$, N_B is the total counts in the background under the peak of interest. The MDL estimated from both spectra are about 3e-4, meaningful in the context of corrosion threshold. The nominal value for slab #3 of 2.5e-3 is 8 times above the MDL. However, the spectra indicated that it was barely detectable, and correspondingly it is much lower than what the simulation predicted. This discrepancy will be investigated in the future.

Unlike reactor based PGAA using gram-sized pressed powder pellets, it is difficult to quantitatively assess bulk concrete chloride levels expressed in terms mass fractions, for which geometry-matching standards are non-existent. Internal ratio methods provide a systematic response of the prompt gamma counts to the chloride

Table 2 Measured Si, Ca, and Cl peak count rates and ratios taken from detector A and B

	Detector A								Detector B							
	Si		Ca		Cl		Cl/(Si + Ca)		Si		Ca		Cl		Cl/(Si + Ca)	
Slab	cps	Rel. unc	cps	Rel. unc	cps	Rel. unc		Rel. unc	cps	Rel. unc	cps	Rel. unc	cps	Rel. unc		Rel. unc
1	2.30	0.02	0.95	0.05	3.30	0.01	1.02	0.05	2.36	0.02	0.92	0.06	3.30	0.02	1.01	0.07
2	4.86	0.01	1.45	0.04	3.51	0.02	0.56	0.05	2.61	0.03	1.14	0.06	2.01	0.03	0.54	0.07
3	1.43	0.02	0.52	0.03	0.21	0.08	0.11	0.09	0.77	0.02	0.29	0.06	0.005	0.46	0.005	0.46
4	3.10	0.01	1.01	0.04	–	–	–	–	1.78	0.02	0.30	0.06	–	–	–	–
5	3.93	0.01	2.23	0.02	–	–	–	–	2.50	0.02	1.04	0.05	–	–	–	–

The relative uncertainty of the count rate is based on 1 s count statistics of the gamma-ray photo peak intensity. The relative uncertainty of the ratio is based on the relative uncertainties from the relevant peaks. For slabs 4, insufficient Cl signal above background was detected. Slab 5 was a control "blank" with no Cl

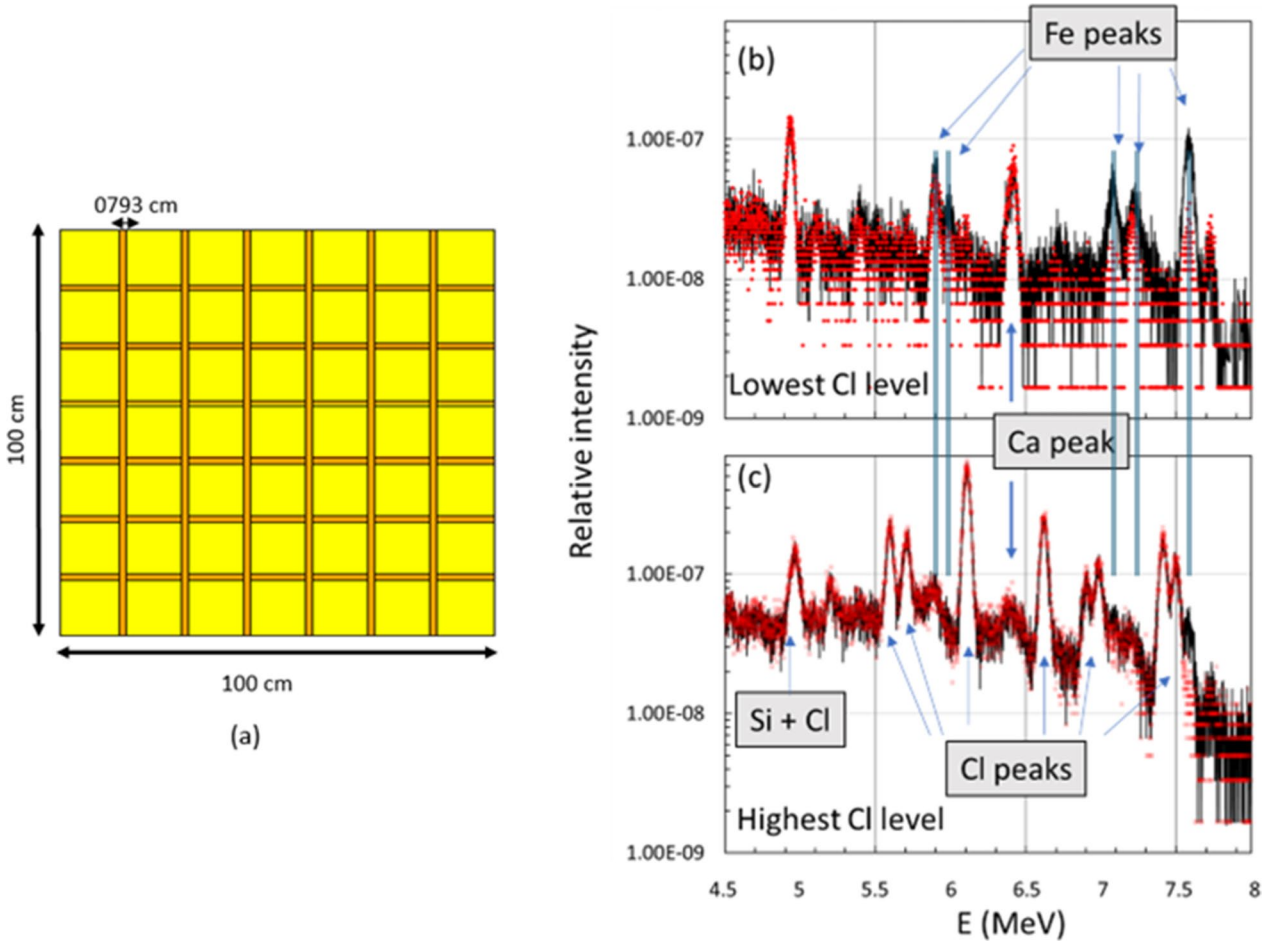

Fig. 6 Effect of added iron bars to simulate reinforcement in concrete. **a** iron bar grid pattern. **b** gamma spectrum obtained at Cl mass fraction of 1e-4. Solid line: with iron bars, points: without iron bars. **c** same as **b**, but at the Cl mass fraction of 0.05. The Fe peaks are obscured by the Cl peaks in (**c**), but the effects of iron bars on the Cl peaks are negligible

level, and relate to a mass fraction given the concrete composition. More often than not, the composition is not well known. Model simulation can be performed using the most common aggregate type and typical concrete recipes. In this work, limited number of measurements was available, due to the low neutron flux of the DD generator. More repeat measurements on different locations of the same slab, or more slabs of the same nominal composition will help establish statistical confidence, and with sufficient simulation and measured data, one can envision employing machine learning to rapidly determine the chloride content in large concrete structures. The goal of this study is to simulate field work situations, where conditions cannot be expected to be well controlled, by using the internal ratio method and a statistical approach. Future effort will address the volume non-uniformity issue by performing measurements at various locations to assess the likelihood of the chloride mass fraction. We will explore coincidence detection schemes with neutron generator pulse mode operation to reduce background and improve the detection limit. Additionally, given the reinforced concrete contains metal rebars, the information from the Fe peaks in the prompt gamma spectrum ("Appendix") from the metal reinforcement inside may be used as an internal depth reference to create a calibration function specific to the source and detector geometry [31], adding depth profiling to the current bulk information. Finally, an "electronic collimation" method based on Compton scattering proposed in [23] will be investigated to obtain spatially resolve chloride distribution, adding information to the depth profile.

Summary

We demonstrated the feasibility of measuring Cl concentration in a large concrete slab using a portable neutron generator and $LaBr_3$ detectors, using the same-side measurement geometry that is likely encountered in a field-test situation, with the concrete also serving as the neutron moderator. Monte Carlo simulation was employed to assess the detector response as a function of Cl concentration using the most common aggregates for meter-sized concrete slabs. The current method can detect sub-percent level Cl that is relevant to corrosion threshold. The detection limit can be improved by using a more intense neutron source, by increasing the number of detectors to cover larger detection volumes, and possibly by a coincidence measurement scheme to reduce the background. For a future field-deployable mobile unit, the neutron yield of the generator and the concrete thickness can be modeled to determine the limit of detection with an on-board simulation module.

Appendix

Simulation of concrete slab with rebars

The current study was conducted on concrete slabs without metal reinforcements (rebar). In reality, rebars are almost always present in a concrete structure. The main concern of chloride diffusion through the concrete is its role in promoting the corrosion of the rebar. To anticipate the field situation where metal reinforcement is present, we investigate whether the Cl peak at 6110 keV could be affected by the Fe peaks in the gamma spectrum. The reinforcement was simulated in MCNP as iron rods and placed in a grid-like manner as shown in Fig. 6, at the bottom of the slab. The rods have a radius of 0.793 cm and are 100 cm long. The Fe peaks are indicated in Fig. 6b. These peaks did not appear in the spectrum without the reinforcement, even though there would be some background due to the minor iron content of the cement. It appears that the reinforcing bars slightly decreased the 6110 keV chloride signal, likely due to the attenuation and/or change of the neutron moderation by the iron bars. However, the effect is negligible.

Acknowledgements This work was partially supported by the NIST Strategic and Emerging Research Initiatives (SERI) Physical Infrastructure program. The concrete slabs were cast by NRMCA and Amde Amde and Jorgomai Ceesay of University of Maryland for an earlier project. We thank Eli Baltic of NIST for assistance during the experimental setup. We are grateful to Jeff Carroll, Chris Chiara, and Jarrod Marsh of the Army Research lab for loaning the $LaBr_3$ detectors and helpful discussions throughout this project.

Declarations

Conflicts of interest The authors have no conflicts of interest in this work.

References

1. Paul RL, Lindstrom RM (2000) Prompt gamma-ray activation analysis: fundamentals and applications. J Radioanal Nucl Chem 243(1):181–189. https://doi.org/10.1023/A:1006796003933/METRICS
2. Lindstrom RM (1993) Prompt-gamma activation analysis. J Res Natl Inst Stand Technol 98(1):127. https://doi.org/10.6028/JRES.098.009
3. Belgya T (2012) Prompt gamma activation analysis at the Budapest research reactor. Phys Procedia 31:99–109. https://doi.org/10.1016/J.PHPRO.2012.04.014
4. Szentmiklósi L, Révay Z, Östör J, Maróti B (2024) Improved analytical workflow for prompt gamma activation analysis. J Radioanal Nucl Chem 333:3325–3333. https://doi.org/10.1007/s10967-023-09071-4
5. Hooton RD (2001) Ion and mass transport in cement-based materials. American Ceramic Society, Westerville
6. Rodrigues R, Gaboreau S, Gance J, Ignatiadis I, Betelu S (2021) Reinforced concrete structures: a review of corrosion mechanisms and advances in electrical methods for corrosion monitoring. Constr Build Mater 269:121240. https://doi.org/10.1016/J.CONBUILDMAT.2020.121240
7. ASTM (2012) ASTM C1152/C 1152M-04 standard test method for acid-soluble chloride in mortar and concrete. ASTM, West Conshohocken
8. Halmen C, Trejo D (2007) Measuring chloride concentrations for various cement-based materials systems. ACI Mater J 104(6):567–574
9. AASHTO (1984) Standard method of sampling and testing, T 260–84, part H-Tests. AASHTO, Washington, DC
10. Torres-Luque M, Bastidas-Arteaga E, Schoefs F, Sánchez-Silva M, Osma JF (2014) Non-destructive methods for measuring chloride ingress into concrete: state-of-the-art and future challenges. Constr Build Mater 68:68–81. https://doi.org/10.1016/j.conbuildmat.2014.06.009
11. Molnár GL, Révay Z, Belgya T (2004) Accurate absolute intensities for the 35Cl(n,γ) reaction gamma-ray standard. Nucl Instruments Methods Phys Res Sect B Beam Interact with Mater Atoms 213:32–35. https://doi.org/10.1016/S0168-583X(03)01529-5
12. Dewey MS, Kessler EG (2024) Precision measurement of fundamental constants using GAMS4. J Res Natl Inst Stand Technol 105(1):11

13. IAEA (2006) Database of prompt gamma rays from slow neutron capture for elemental analysis. International Atomic Energy Agency, Vienna
14. Livingston RA, Sridhar P, Berke NS, Amde AM, Chen-Mayer HH (2024) Measurement of chloride in concrete by prompt-gamma neutron activation. Am Concr Inst Mater J 121(5):13–22. https://doi.org/10.14359/51742035
15. Chen-Mayer HH, Berke NS, Livingston RA (2023) Pgaa measurement of chloride diffusion profiles in concrete cylinders. J Radioanal Nucl Chem 332:5239–5245. https://doi.org/10.1007/s10967-023-09023-y
16. Wakabayashi Y, Hashiguchi T, Yoshimura Y, Mizuta M, Ikeda Y, Otake Y (2020) Study of a collimation method as a nondestructive diagnostic diagnostic technique by PGNAA for salt distribution in concrete structures at RANS. EPJ Web Conf 231:05007. https://doi.org/10.1051/EPJCONF/202023105007
17. Wakabayashi Y et al (2018) A study on the non-destructive detection of salt in concrete using neutron-captured prompt-gamma rays at RANS. Plasma Fusion Res 13:2404052. https://doi.org/10.1585/pfr.13.2404052
18. Collico Savio DL, Mariscotti MAJ, Guevara SR (1995) Elemental analysis of a concrete sample by capture gamma rays with a radioisotope neutron source. Nucl Instrum Methods Phys Res B Beam Interact Mater Atoms 95:379–388
19. Saleh HH, Livingston RA (2000) Experimental evaluation of a portable neutron-based gamma-spectroscopy system for chloride measurements in reinforced concrete. J Radioanal Nucl Chem 244(2):367–371. https://doi.org/10.1023/A:1006787626016
20. Mohamed AB, Al-Sheikhly M, Livingston R, Saleh H (2008) Monte Carlo simulations of a portable prompt gamma system for nondestructive determination of chloride in reinforced concrete. Nucl Instruments Methods Phys Res Sect B 266(15):3397–3405. https://doi.org/10.1016/J.NIMB.2008.04.021
21. Yan M, Wakabayashi Y, Takamura M, Ikeda Y, Otake Y (2022) Optimization study of chlorine detection sensitivity in concrete based on prompt gamma analysis using ^{252}Cf neutron source. Appl Radiat Isot 188:110393. https://doi.org/10.1016/J.APRADISO.2022.110393
22. Livingston RA, Al-Sheikhly M, Mohamed AB (2010) Numerical simulation of the PGNA signal from chlorine diffusion gradients in concrete. Appl Radiat Isot 68(4–5):679–682. https://doi.org/10.1016/J.APRADISO.2010.01.029
23. Livingston RA, Al-Sheikhly M, Made AM (2014) Development of a 2nd generation neutron-based detector for chloride in concrete final report for highway IDEA project 136. Accessed from www.trb.org/idea
24. Naqvi AA, Nagadi MM, Al-Amoudi OSB (2004) Elemental analysis of concrete samples using an accelerator-based PGNAA setup. Nucl Instrum Methods Phys Res Sect B 225(3):331–338. https://doi.org/10.1016/J.NIMB.2004.04.170
25. Naqvi AA, Maslehuddin M, Kalakada Z, Al-Amoudi OSB (2014) Prompt gamma ray evaluation for chlorine analysis in blended cement concrete. Appl Radiat Isot 94:8–13. https://doi.org/10.1016/J.APRADISO.2014.06.011
26. Naqvi AA, Kalakada Z, Al-Matouq FA, Maslehuddin M, Al-Amoudi OSB, Ur-Rehman K (2012) Prompt gamma-ray analysis of chlorine in superpozz cement concrete. Nucl Instruments Methods Phys Res Sect A 693:67–73. https://doi.org/10.1016/J.NIMA.2012.06.059
27. Naqvi AA, Nagadi MM, Al-Amoudi OSB (2006) Prompt gamma analysis of chlorine in concrete for corrosion study. Appl Radiat Isot 64(2):283–289. https://doi.org/10.1016/J.APRADISO.2005.07.015
28. Werner CJ et al (2018) MCNP ® user's manual code version 6.2. Los Alamos National Security LLC, Los Alamos
29. Rooney B, Garner S, Felsher P, Karpius P (2018) PeakEasy 4.98 [Computer Program], Los Alamos National Laboratory, Release LA-CC-13-040. https://PeakEasy.lanl.gov.
30. Soppera N MeshTal viewer. Nuclear Energy Agency, https://www.oecd-nea.org/jcms/pl_37329/.
31. Linvingston RA (1993) Standardization of the neutron probe for the assessment of masonry deterioration. Appl Radiat Isot 44(IO/II):1285–1300